A new laboratory apparatus for the measurement of seismic dispersion under deviatoric stress conditions.

Dawid Szewczyk[1], Andreas Bauer[1,2] & Rune M. Holt[1]

[1.] *Norwegian University of Science and Technology (NTNU), Department of Petroleum Technology & Applied Geophysics, 7491, Trondheim, Norway.*

[2.] *SINTEF Petroleum Research, Formation Physics, 7465, Trondheim, Norway.*

Contact email: dawid.szewczyk@ntnu.no

Abstract

A better understanding of seismic dispersion and attenuation of acoustic waves in rocks is important for quantitative interpretation of seismic data, as well as for relating seismic data, sonic-log data, and ultrasonic laboratory data. In the present work, a new laboratory setup is described, allowing for combined measurements of quasi-static deformations of rocks under triaxial stress, ultrasonic velocities, and dynamic elastic stiffness (Young's modulus and Poisson's ratio) at seismic frequencies. The setup has been used mainly for the study of shales. For such rocks, it is crucial that the saturation of the samples is preserved, which requires fast sample mounting. Design of our setup together with a technique that was developed for rapid mounting of strain gages onto the sample and subsequent sealing of the sample allows for sample preservation, which is of particular importance for shales. The performance of the new experimental setup and sample-mounting procedure is demonstrated with test materials (Aluminum and PEEK) as well as two different shale types (Mancos shale and Pierre shale). Furthermore, experimental results are presented that demonstrate the capability of measuring the impact of saturation, stress and stress-path on seismic dispersion. For the tests with Mancos and Pierre shale, large dispersion (up to 50% in Young's modulus normal to bedding) was observed. Increased water saturation of Mancos shale results in strong softening of the rock at seismic frequencies, while hardening is observed at ultrasonic frequencies due to an increase in dispersion, counteracting the rock softening. Poisson's ratio of Mancos shale strongly increases with level of saturation but appears to be nearly frequency independent. We have found that the different types of shale exhibit different stress sensitivities during hydrostatic loading, and also that the stress sensitivity is different at seismic and ultrasonic frequencies.

1   Introduction

Rock physics models for the quantitative interpretation of seismic and sonic data are often developed based on ultrasonic data obtained with core plugs in the laboratory. It is known that fluid saturated sedimentary rocks are dispersive in nature (e.g. Batzle et al. 2005; Batzle et al. 2006; Pimienta et. al. 2015; Duranti et. al. 2005). Therefore, when comparing field and laboratory measurements, seismic dispersion, i.e. the frequency dependence of acoustic velocities, has to be taken into account. Frequency dependent properties of rocks result from elastic wave induced fluid movements in the pore space. Different theories on the frequency dependence of wave propagation and its underlying mechanisms have been proposed, however their validation remains difficult because of the lack of experimental data (Müller et al., 2010). Therefore, systematic laboratory studies performed under well-defined and controllable conditions and with well characterised samples are of great value. Over the last few decades, several experimental techniques for measuring seismic dispersion and attenuation have been developed, e.g. the forced oscillatory method (Spencer 1981). However, the number of experimental setups for measuring seismic dispersion in porous rocks as well as the amount of published data are still small (e.g. Adam et al. 2006; Batzle et al. 2001; Tisato and Madonna 2012; Mikhaltsevitch et al. 2014; Pimienta et al. 2015).

In this work, a new experimental setup has been developed that allows for combined measurements of quasi-static rock deformation, ultrasonic velocities, and dynamic elastic stiffness at seismic frequencies under pore pressure and deviatoric stress. Experiments have been performed with both standard samples (Aluminum type 7075, and polyether ether ketone, PEEK), as well as with two different shale outcrops (Mancos shale and Pierre shale). New procedures were developed for strain-gage mounting and sample sealing that allow minimizing sample-mounting time and thus exposure to air. This is essential for investigating shale samples. Taking into account the limited number of publications describing dispersive properties of shales and their impact on interpretation of seismic and sonic data (Hofmann 2006; Delle Piane et al. 2014; Suarez-Rivera et al.2001; Sarker and Batzle 2010; Duranti, Ewy, and Hofmann 2005) there is a need for further research on this topic.

After a description of the experimental setup (Chap. 2) and experimental procedures (Chap. 3), examples are given for different applications of the new setup, including effects of stress and stress path on seismic dispersion, as well as water saturation effects on static and dynamic stiffnesses of shales (Chap. 4).

2   Experimental set-up

In this section, the design of a new triaxial compaction cell (placed at Formation Physics laboratory of SINTEF Petroleum Research) will be described. The cell is used for measuring quasi-static deformations of core plugs under stress, as well as dynamic Young's modulus and Poisson's ratio, intrinsic attenuation at seismic frequencies (0.1 Hz – 200 Hz), and p- and s-wave ultrasonic velocities at different stresses and pore pressures. The ambition was to establish a technique for complete characterization of the frequency-dependent elastic properties of anisotropic rocks under stress. The compaction cell is designed for 1"-diameter samples, and a maximum confining pressure of 70MPa. To determine elastic parameters at seismic frequencies the forced-oscillator concept was utilized (Spencer 1981), with small axial strain oscillations. Conceptually, our setup is similar to the apparatus at Colorado School of Mines (Batzle et al., 2006) with few modifications that allow for faster sample mounting, independent stress control in axial and radial directions and quasi-static measurements. In our design we have replaced the shaker imposing small oscillating force on the sample by a piezoelectric actuator integrated in the sample stack. Indirect force modulation measurements are replaced by direct force measurements using a piezoelectric force sensor. Furthermore, design of our sample holder together with different sealing method and sample/strain gage fitting technique allows for mounting the sample within a few hours. Detailed description of the procedure will be given in Section 3.1. A schematic drawing and a photograph of the sample stack is shown in Figure 1. The sample stack consists of the sample in between two steel endcaps, an aluminum piece equipped with a pair of strain gages, a piezoelectric force sensor (Kistler), a piezoelectric actuator (PI), and an internal load cell (MetaRock). The entire column is mounted on the base flange of the compaction cell. The compaction cell is placed inside a mechanical loading frame (MTS) that exerts axial force on

the sample stack through a piston fed through the top flange of the compaction cell. The base flange is equipped with both 4-pin and coaxial electric feedthroughs, as well as fluid lines for confining and pore pressure control. For the measurement of the static axial deformation of the sample, three linear variable displacement transducers (LVDT) are mounted in between the endcaps. The whole compaction cell may be placed inside an oven for compaction measurements at elevated temperature.

The whole setup may be divided into four units: a seismic-frequency unit, an ultrasonic unit, a static-deformation unit, and a pore-pressure unit that will be described in more detail below.

[Figure 1 about here]

2.1 Static-deformation unit

The static-deformation unit consists of the loading frame, confining-pressure control, the three LVDTs, the strain gages attached to the sample, and the internal load cell. The confining pressure applied to the sample is controlled by a Quizix pump allowing for accurate pressure control up to 50 MPa. Axial force is exerted by the MTS loading frame allowing for sub-Newton force control (using an external load cell).

The axial strain of the sample is measured by averaging three LVDTs that are distributed equally around the circumference of the sample. Axial strain is also measured by two axial-strain gage pairs attached to the sample. While the strain gages measure the strain locally (over a length of several mm), the LVDTs measure the strain of the whole sample. A large deviation of the two independently measured axial strains indicates the presence of large heterogeneities in the sample, or some errors in the strain-gage or LVDT readings. The radial strain of the sample is measured along two orthogonal directions by two radial-strain gage pairs attached to the sample. The Poisson's ratios for these two directions are obtained from the ratio of axial strain to the respective radial strain. The axial deviatoric stress acting on the sample is measured by the internal load cell. For axial loading (triaxial

loading), Young's modulus is determined from the ratio of the change in axial stress to the change in axial strain.

2.2   Ultrasonic unit

Compressional (P) and shear (S) wave ultrasonic velocities along the sample axis are measured by applying the typical pulse-transmission technique, using two pairs of in-house built ultrasonic transducers embedded in the top and bottom endcaps. Both p- and s-wave piezoelectric crystals have a center frequency of 500 kHz.

2.3   Low-frequency unit

The low-frequency unit is composed of a displacement actuator, the force sensor, four sealed foil strain-gage pairs attached to the sample (the same gages are used for quasi-static deformation measurements), and 5 digital lock-in amplifiers (Stanford Research). A sinusoidal electric signal is generated by one of the lock-in amplifiers, amplified and applied to the piezoelectric actuator placed in the column. Typical actuator displacement amplitudes are of the order of 20-75nm, resulting in sample strains of $< 10^{-6}$ measured by the strain gages. The displacement modulation results in an axial-force modulation that is measured with the piezoelectric force sensor. Both strain-gage signals (2 axial and 2 radial channels) and force signal are measured by phase-sensitive lock-in amplifiers. From the force, F, and strain, ε, modulation amplitudes, both Young's modulus, E, and Poisson's ratios, ν, can be calculated:

$$E = \frac{\Delta\sigma_{ax}}{\Delta\varepsilon_{ax}} = \frac{\Delta F_{ax}}{A\cdot\Delta\varepsilon_{ax}} \text{ , and } \nu = -\frac{\Delta\varepsilon_{rad}}{\Delta\varepsilon_{ax}} \tag{1}$$

A is the cross-section area of the sample, and the indices *ax* and *rad* indicate axial and radial direction, respectively. Energy dissipation in the sample (intrinsic attenuation) results in a phase shift between force and strain signals. However, since different electronic circuitry is used for the force sensor (manufacturer's control unit) and the strain gages (Wheatstone bridges), electronics-induced frequency-dependent phase shifts were found to be larger than the phase shifts induced by

attenuation in the (rock) sample, which makes accurate attenuation measurements difficult. To improve attenuation measurements, a cylindrical aluminum piece was added to the sample stack onto which a strain-gage pair was mounted (foil gages used initially will be replaced by semiconductor gages with higher gage factors to give more stable strain signals). Since aluminum is non-dispersive, its strain is in phase with the applied force, and the attenuation in the sample can be obtained from the phase shift between the strain-gage signals of the sample and the aluminum piece. This technique has been introduced and successfully applied by Batzle et al. (2005). It should be noted that phase shifts would also occur close to mechanical resonances of the sample stack. For the present setup, an impact of mechanical resonances on seismic dispersion measurements has been observed for frequencies > 150-200 Hz.

2.4   Pore-pressure unit

The pore pressure unit is composed of two pore-fluid lines connected to the two endcaps, small-volume pressure gages, pneumatic valves, and a Quizix pump for pore-pressure control. For low-permeability shale samples, efficient pore-pressure control requires side drainage. To this end, metal mesh is wrapped around the sample (with slots at the positions of the strain gages) and accessed by the pore fluid through radial holes in the endcaps. As pointed out by White (1986), and experimentally proven by Dunn (1987), macroscopic pore fluid flow through the free sample's boundary may lead to significant errors during low frequency experiments. It is therefore crucial to minimize the pore-fluid volume outside the sample (dead volume). In the present setup, small-diameter pore-fluid lines were used, and both pore-pressure transducers and pneumatic valves were positioned next to the cell. In this way, the dead volume could be reduced to 0.5 ml, which is small enough for most applications. It should be noted that for shale measurements, the valves can remain open since the permeability of shales is low enough (nano-Darcy range) to prevent drainage even for frequencies as low as 0.1 Hz.

2.5   Possible sources of experimental errors

Errors in the dynamic strain, measured locally on the sample, may arise due to (i) sample bulging, (ii) possible small misalignment of the stack (which would decrease with increasing confining pressure) that could result in a non-homogeneous stress and strain distribution in the sample, (iii) a heterogeneous sample exhibiting local strain variations on a scale larger than the size of the strain gages, or (iv) non-parallel alignment of the strain gages with respect to the sample axis. Electronic noise is another error source. It can also not be ruled out that friction between the rubber jacket and the oil used for applying confining pressure cause some energy dissipation. Furthermore, for anisotropic samples, sample-orientation errors would result in systematic errors of the derived stiffness parameters. Along the same line, errors in the ultrasonic s-wave velocities would arise by misalignment of the ultrasonic s-wave transducers with respect to the bedding orientation Quantifying all possible errors is a demanding task. Nevertheless, total errors can be estimated from measurements with non-dispersive standard materials for which the stiffness is known. In case of aluminum, the experimental errors for Young's modulus and Poisson's ratio did not exceed 5%.

3 Experimental procedures

For the measurements of shales (but also other rock samples), it is crucial that the saturation of the rock sample is preserved. It is therefore important to keep the time the samples are exposed to air during mounting as short as possible. To this end, experimental procedures were developed that allowed for sample mounting within less than 1 hour. Two of the procedures are described in more detail in the following.

3.1 Strain gage mounting

Instead of gluing the strain gages to the sample's surface, which takes significant time, the gages were taped onto the surface. The purpose of the tape is to keep the gages in place during mounting of the rubber sleeve; the actual mechanical coupling between gage and sample is provided by the confining pressure. In order to prove that non-glued gages give the same result as glued gages, experiments were performed with both PEEK, Aluminum and partially saturated Mancos shale where

non-glued gages were used in a first experiment, and glued gages (the same gages as before) in a repeat experiment under identical conditions. For all tested specimens, the obtained Young's moduli deviated on average by less than 1.5% with the maximum deviation of 2.5% (in case of aluminum) and Poisson's ratios deviated by less than ±0.02 (the results are shown in Figure 2). In fact, in some cases, the measured Young's moduli were even slightly smaller for the non-glued gages than for the glued gages; slippage of the non-glued gages would result in smaller strains and thus higher Young's moduli. In order to make a final conclusion about this mounting method, further detailed studies will be performed in the near future, addressing effects of saturation, saturation fluids, confining pressure, and temperature. However, from our current experience, non-glued gages can be used for both dynamic and quasi-static deformation measurements over several hours or days.

[Figure 2 about here]

3.2   Sample mounting

When mounting the sample in between the endcaps and sealing it with a rubber sleeve, the 16 wires from the 8 strain gages mounted onto the sample have to be fed out. This can be achieved by replacing the O-ring of the bottom endcap by two layers of vulcanizing tape, with the strain-gage wires embedded in between the layers. Each layer of vulcanizing tape was made by wrapping a thin strip of tape a couple of time around the endcap, the first one filling the O-ring notch of the endcap. This technique results in good seals for oil as a confining fluid. It needs to be checked whether the seals are also gas tight.

4   Results and Discussion

4.1   Test samples

Aluminum (type 7075) and PEEK were used to test the new experimental setup. Both materials are homogenous and isotropic. Aluminum is non-dispersive, which makes it a good test material for dynamic-stiffness measurements: both Young's modulus and Poisson's ratio are frequency

independent. Also PEEK, being much softer than aluminum, has been shown to exhibit vanishing or small dispersion. Results of the test measurements are shown in Figure 3. The absence of dispersion is confirmed for both aluminum and PEEK, and the obtained Young's moduli (Figure 3a) and Poisson's ratios (Figure 3b) for both seismic and ultrasonic frequencies (black open markers) are in good agreement with values obtained in previous ultrasonic tests (filled small symbols at 500 kHz) using different equipment. It should be noted that for the seismic-frequency measurements, no adjustments of calibration constants were done; gage factors provided by the strain-gage manufacturer as well as the factory calibration of the force sensor were used.

[Figure 3 about here]

4.2   *Seismic-frequency measurements with anisotropic samples*

Generally, in anisotropic, elastic materials stress σ_{ij} and strain ε_{kl} tensors are related by Hooke's law which, with the use of Einstein's summation convention, may be written as:

$$\sigma_{ij} = C_{ijkl}\varepsilon_{kl} \tag{2}$$

where C_{ijkl} represents the elastic stiffness matrix.

For transversely isotropic (TI) materials, the stiffness matrix can be written in Voigt notation with 5 independent stiffness parameters as (e.g. Nye 1985):

$$C_{ij} = \begin{bmatrix} C_{11} & C_{11} - 2C_{66} & C_{13} & 0 & 0 & 0 \\ C_{11} - 2C_{66} & C_{11} & C_{13} & 0 & 0 & 0 \\ C_{13} & C_{13} & C_{33} & 0 & 0 & 0 \\ 0 & 0 & 0 & C_{44} & 0 & 0 \\ 0 & 0 & 0 & 0 & C_{44} & 0 \\ 0 & 0 & 0 & 0 & 0 & C_{66} \end{bmatrix} \tag{3}$$

From our low frequency experiments, the 5 independent stiffness parameters C_{11}, C_{33}, C_{44}, C_{66}, and C_{13}, can be obtained from measurements with three different sample orientations. In the present study, measurements were done with cylindrical samples whose axis had an angle of 0°, 45°, and 90° with respect to the bedding plane (TI symmetry plane). The following Young's moduli and Poisson's ratios were obtained with the seismic-frequency measurements: E_V and ν_{VH} for the 0° sample, E_H,

ν_{HH}, and ν_{HV} for the 90° sample, and E_{45} for the 45° sample (in total 6 parameters). For TI media, the following relation holds:

$$\frac{\nu_{VH}}{E_V} = \frac{\nu_{HV}}{E_H}$$
(4)

This relation can be used to verify TI symmetry but it can also be used to verify experimentally determined values if it is known that a sample represents TI symmetry.

Figure 4 shows Young's moduli and Poisson's ratios at seismic frequencies measured with Mancos shale. Mancos shale is an outcrop that is considered an analogue to gas shales (Holt et. al. 2013).

[Figure 4 about here]

The results reveal a relatively large dispersion in Young's modulus and nearly no dispersion in Poisson's ratio in the seismic frequency range (1 – 155 Hz). The data also reveals stiffness anisotropy. Young's modulus measured for loading parallel to bedding, E_H (90° sample), is significantly higher than that for loading perpendicular to bedding, E_V (0° sample). As expected for anisotropic media, Poisson's ratio obtained with the 0° sample, ν_{VH}, lies in between the two Poisson's ratios obtained with the 90° sample, ν_{HH} and ν_{HV}. Interestingly, within the error of the measurements, equation (4) is confirmed by the measurements (see open squares in Figure 4a). This indicates that Mancos shale can be described as transversely isotropic medium. The fact that $(E_H/E_V)/(\nu_{HV}/\nu_{VH}) \approx 1$ is frequency independent gives confidence in the validity of the experimental technique.

4.3   Dispersion in shales – effects of stress, stress path and saturation

A series of experiments have been performed in which stress, stress path and saturation effects on seismic dispersion in different shale types were investigated. Here, only selected results, summarized in Figure 5, will be presented in order to demonstrate the capabilities of the new experimental setup. The experiments will be described in more detail in forthcoming publications.

[Figure 5 about here]

In Figure 5(a,b), the saturation dependence of Young's modulus, E_V, and Poisson's ratio, ν_{VH}, of Mancos shale is shown by comparing data obtained with samples stabilized in environments of 11% and 100% relative humidity (RH), respectively. As-received samples (corresponding to around 86% RH) were placed in the desiccators in which the RH was controlled by saturated solutions of different types of salts (Greenspan 1977). Actual RH was verified by hygrometers inside the desiccators. Specimens were stabilizing under room temperature and their weight was controlled on daily basis. The sample exposed to 100% RH was gaining weight, while the others were losing weight. Experiments were performed after the weight of samples did not change by more than 0,01g over the course of 1 week. In case of Mancos samples it took around 4-5 weeks. Both tests were carried out under deviatoric stress condition with 17 MPa confining stress, and 26 MPa axial stress. Both Young's modulus and Poisson's ratio exhibit strong saturation sensitivity. Large seismic dispersion of > 50% in E_V between seismic and ultrasonic frequencies is observed for the 100% RH sample, while the 11% RH sample exhibits only small dispersion. It is interesting to note that the change in saturation affects the Young's modulus differently at seismic and ultrasonic frequencies: An increase in water saturation results in a strong softening of the shale at seismic frequencies, while it causes stiffening at ultrasonic frequencies as a result of strongly increased dispersion (this effect will be discussed in details in the forthcoming paper). Also Poisson's ratio, not exhibiting any sizable dispersion, is strongly affected by saturation changes. It increases from about 0.08 at 11% RH to about 0.3 for the 100% RH sample.

The capability of measuring stress-induced Young's modulus changes as small as < 0.3 GPa is demonstrated in Figure 5(c-e). In Figure 5(c) and (d), hydrostatic-stress sensitivities of Young's modulus, E_V, of Mancos shale and Pierre shale are presented. The data was obtained with an as-received Mancos shale sample (corresponding to 86% RH), and a Pierre-shale sample stabilized over a period of 6 weeks in a 75% RH environment (applying the same method as for Mancos shale, with the difference that the as-received Pierre-shale samples were fully saturated). Experiments were carried out without pore-pressure control. Both the Mancos-shale sample and Pierre-shale sample

were exposed to three different confining pressures: 5 MPa, 10 MPa and 20 MPa for Mancos shale, and 3.5 MPa, 13.5 MPa and 23.5 MPa for Pierre shale. A constant additional stress (2 MPa for Mancos shale, and 1.5 MPa for Pierre shale) was applied in axial direction in order to improve the signal quality of the low-frequency data. It is clearly seen that the stress sensitivities of Pierre and Mancos shales are different. While Mancos shale exhibits relatively small variations in Young's moduli both at seismic and ultrasonic frequencies (changes are of the order of 0.15%/MPa), Pierre shale shows a significantly higher sensitivity of about 0.72%/MPa. It is important to note that for both shale types, the absolute Young's modulus changes are similar at seismic and ultrasonic frequencies. Given the large dispersion, the relative changes are higher at seismic frequencies, though.

Finally, in Figure 5(e), the impact of constant-mean-stress loading on the Young's modulus, E_V, is shown for fully saturated Pierre shale. The corresponding stress path is shown in Figure 5(f). For this test, a preserved Pierre shale sample was exposed to 3.5% NaCl brine, and a pore pressure of 2 MPa was applied. Seismic-dispersion measurements were carried out after consolidation at a confining stress of 19.5 MPa and an axial stress of 21 MPa. Subsequently, the axial stress was increased to 26 MPa, and the confining stress was reduced to 17 MPa, before another seismic-dispersion measurement was done. Finally, the static Young's modulus was measured (lower solid circle in Figure 5e) during a triaxial unloading step (the axial stress was reduced from 26 MPa to 17 MPa). A quasi-static Young's modulus (upper solid circle in Figure 5e) was derived by extrapolating the compressibility, $d\varepsilon_{ax}/d\sigma_{ax}$, during unloading to zero strain (this method is described in Fjær et al., 2013). The reason for plotting the quasi-static Young's modulus at a frequency of 1 Hz is that the strain rate during unloading corresponds approximately to the strain rate of the dynamic measurements at 1 Hz. This zero-strain extrapolated Young's modulus agrees surprisingly well with the low-frequency limit of the dynamic Young's modulus, which indicates that the difference between static and dynamic Young's modulus at a given frequency is due to both a strain effect (plasticity effect) and a dispersion effect (Holt et al., 2015).

5   Conclusion

A new apparatus for combined static-compaction, ultrasonic and dynamic stiffness measurements at seismic frequencies under triaxial stress conditions has been described. Measurements have successfully been carried out with aluminum and PEEK samples that demonstrate in particular the applicability of novel sample-mounting procedures that have been developed and that have a potential to minimize sample-mounting time and thus exposure to air. The capability of measuring the elastic properties of anisotropic samples at seismic frequencies was demonstrated on Mancos shale. Furthermore, selected results obtained with Mancos shale and Pierre shale were presented that demonstrated the capability of the new experimental setup to study the impact of saturation, stress, and stress path on seismic dispersion, as well as the relation of static to dynamic stiffness. For all experiments done with shales we have observed frequency dependent effects which causes differences between seismic and ultrasonic regimes to be as high as 50% in Young's modulus. Increased saturation of Mancos shale results in strong softening of the samples in the seismic regime in addition to strongly increased dispersion, causing stiffening at ultrasonic frequencies. Poisson's ratio of Mancos shale appears frequency independent and strongly increases with saturation level. Hydrostatic loading of Mancos shale and Pierre shale demonstrates different stress sensitivities of these two rock types. Pierre shale is around 5 times more sensitive to the applied stress than Mancos (showing changes of the order of 0.72%/MPa as compared to 0.15%/MPa for Mancos). The absolute changes of Young's modulus are similar at seismic and ultrasonic frequencies, however due to large dispersion relative changes of E_v are smaller in the ultrasonic regime. Pierre shale properties obtained during constant-mean-stress loading reveals that the shales are sensitive to the loading path. Measuring both quasi-static and multi-frequency dynamic responses within a single experiment shows that the differences between static and dynamic moduli are due to both strain-amplitude effect and dispersion.

6   Acknowledgments

References

Adam L., Batzle M. and Brevik I. 2006. Gassmann's fluid substitution and shear modulus variability in carbonates at laboratory seismic and ultrasonic frequencies. *GEOPHYSICS* 71,(6), F173-F183.

Batzle M., Hofmann R., Han D. and Castagna J. 2001. Fluids and frequency dependent seismic velocity of rocks. *The Leading Edge* 20,(2), 168-171.

Batzle M., Hofmann R., Prasad M., Kumar G., Duranti L. and Han D. 2005. Seismic Attenuation: Observations and Mechanisms. 2005 SEG Annual Meeting, 6-11 November, Houston, USA, SEG-2005-1565.

Batzle M., Han D. and Hofmann R. 2006. Fluid mobility and frequency-dependent seismic velocity — Direct measurements. *GEOPHYSICS* 71, N1-N9.

Cole K.S., Cole R.H. 1941. Dispersion and Absorption in Dielectrics - I Alternating Current Characteristics. *The Journal of Chemical Physics* 9, 341–352.

Delle Piane C., Sarout J., Madonna C., Saenger E. H., Dewhurst D. N., Raven M. 2014. Frequency-dependent seismic attenuation in shales: experimental results and theoretical analysis. *Geophysical Journal International* 198, 504-515.

Dunn K. J. 1987. Sample boundary effect in acoustic attenuation of fluid-saturated porous cylinders. *The Journal of the Acoustical Society of America* 81, 1259-1266 .

Duranti L., Ewy R. and Hofmann R. 2005. Dispersive and Attenuative Nature of Shales: Multiscale and Multifrequency Observations. 2005 SEG Annual Meeting, 6-11 November, Houston, USA, SEG-2005-1577.

Fjær E., Stroisz A.M. and Holt R.M. 2013. Elastic Dispersion Derived from a Combination of Static and Dynamic Measurements. *Rock Mechanics and Rock Engineering* 46,(3), 611-618.

Greenspan L. 1977. Humidity fixed points of binary saturated aqueous solutions. *Journal of Research of the National Bureau of Standards*.Vol. 81A, No. 1.

Hofmann R. 2006. Frequency dependent elastic and anelastic properties of clastic rock. PhD thesis at Colorado School on Mines, Golden, CO, USA.

Holt R.M., Bauer A., Fjær E., Nes O.L. 2013. Rock Physics Analysis of a Gas Shale Analogue. The 2nd International Workshop on Rock Physics. 4-9 August 2013, Southampton, United Kingdom.

Holt R.M., Bauer A., Fjaer E., Stenebråten J.F., Szewczyk D., Horsrud P. 2015. Relating Static and Dynamic Mechanical Anisotropies of Shale. 49th U.S. Rock Mechanics/Geomechanics Symposium, 28 June-1 July, San Francisco, California, ARMA-2015-484

Mikhaltsevitch V., Lebedev M. and Gurevich B. 2014. A laboratory study of low-frequency wave dispersion and attenuation in water-saturated sandstones. *The Leading Edge* 33,(6), 616-622.

Müller, T.M., Gurevich, B., and Lebedev, M. 2010. Seismic wave attenuation and dispersion resulting from wave-induced flow in porous rocks – a review. *Geophysics* 75, 75A147-75A164.

Nye J.F. 1985. Physical Properties of Crystals: Their Representation by Tensors and Matrices. Oxford University Press. ISBN: 9780198511656.

Pimienta L., Fortin J. and Gueguen Y. 2015. Experimental study of Young's modulus dispersion and attenuation in fully saturated sandstones. *GEOPHYSICS* 80,(5), L57-L72.

Sarker, R. and Batzle, M. (2010) Anisotropic elastic moduli of the Mancos B Shale- An experimental study. SEG Abstract 2010; 4 pp.

Spencer J. W. 1981. Stress relaxations at low frequencies in fluid-saturated rocks: Attenuation and modulus dispersion. Journal of Geophysical Research: Solid Earth 86,(B3), 1803-1812.

Suarez-Rivera, R., Willson, S., Nakagawa, S., Nes, O. M., and Liu, Z. (2001) Frequency scaling for evaluation of shale and mudstone properties from acoustic velocities. AGU 2001 Fall Meeting, San Francisco, December 10-14, Paper No. T32E-0924.

Tisato N. and Madonna C. 2012. Attenuation at low seismic frequencies in partially saturated rocks: Measurements and description of a new apparatus. *Journal of Applied Geophysics* 86, 44-53.

White J. E. 1986. Biot-Gardner theory of extensional waves in porous rods. *GEOPHYSICS* 51,(3), 742-745.

List of figures

seismic and ultrasonic frequencies for hydrostatic loading (5, 10, and 20 MPa) at a constant additional axial stress of 2 MPa. (d) Stress sensitivity of Young's modulus, E_V, of partially saturated Pierre shale (stabilized in 75% RH) at seismic and ultrasonic frequencies for hydrostatic loading (3.5, 13.5, and 23.5 MPa) at a constant additional axial stress of 1,5 MPa. (e) Impact of constant-mean-stress loading on the Young's modulus, E_V, of fully saturated Pierre shale at seismic and ultrasonic frequencies. The stress path used in this experiment is shown in (f). Also shown in (e) is the static Young's modulus obtained from triaxial unloading, and the zero-strain extrapolation of the static Young's modulus (Fjær et al. 2013). Solid lines in (a-e) show manual Cole-Cole fits to the experimental data (Cole and Cole 1941).

Figure 1: (a,b) Schematic drawings of the experimental setup (a) and the sample with attached foil strain gages for measuring strain in axial and radial direction (b). Indicated on the drawings are: piston (A), pressure vessel (B), linear variable displacement transducer (LVDT) for measuring axial quasi-static deformations (C), top and bottom endcaps with embedded compressional and shear wave transducers and pore-fluid lines (D), adapter plates holding the LVDTs (E), aluminum standard with attached strain gages for phase shift measurements (F), piezoelectric force sensor for measuring force modulations at seismic frequencies (G), piezoelectric actuator for generating displacement modulations at seismic frequencies (H), internal load cell for measuring static deviatoric stress (I), strain gages attached to sample for static and quasi-static strain determination (J), and pore-fluid lines (K). (c) A photograph of the sample stack. Not shown in the drawings and the photograph is the rubber sleeve around the sample that seals the sample from the oil in the cell used for applying confining stress.
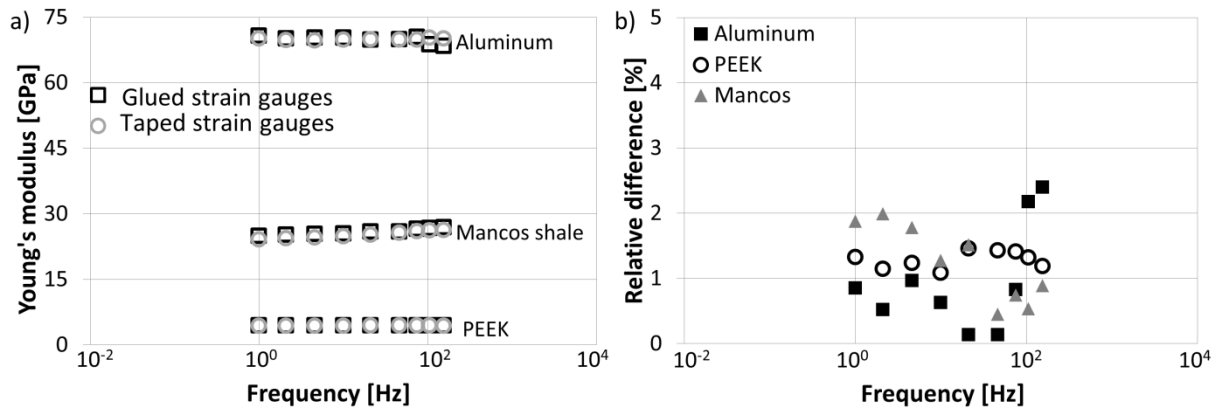
Figure 2: (a) Young's modulus of Aluminum, PEEK and Mancos shale measured at seismic frequencies with non-glued (circles) and glued strain gages (squares). The measurements were done under a confining pressure of 17 MPa and an axial stress of 26 MPa. (b) Relative difference between Young's moduli obtained with glued and non-glued strain.
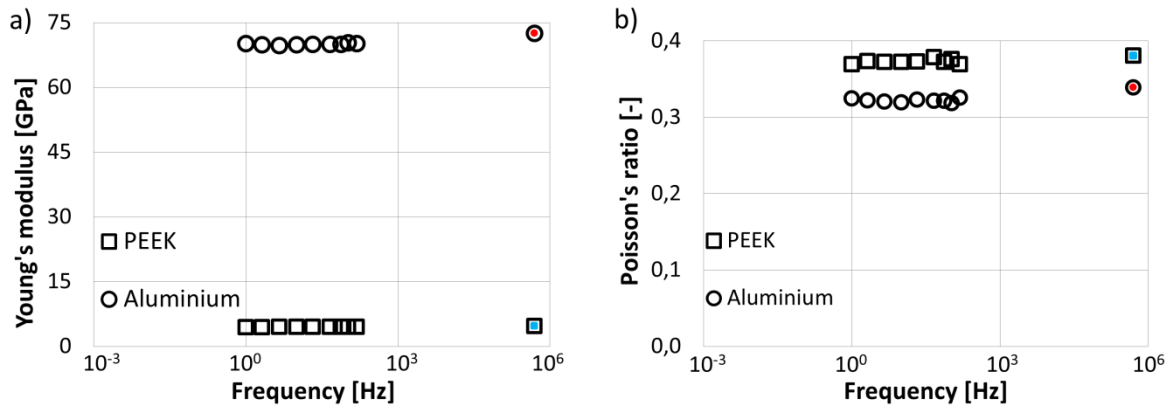
Figure 3: Frequency dependent Young's modulus (a) and Poisson's ratio (b) of aluminum 7075 measured at a confining stress of 10 MPa and an axial stress of 20 MPa, and PEEK measured at a confining stress of 17 MPa and an axial stress of 26 MPa. Small colour symbols at 500 kHz represents data obtained outside our low-frequency setup with the use of different equipment.
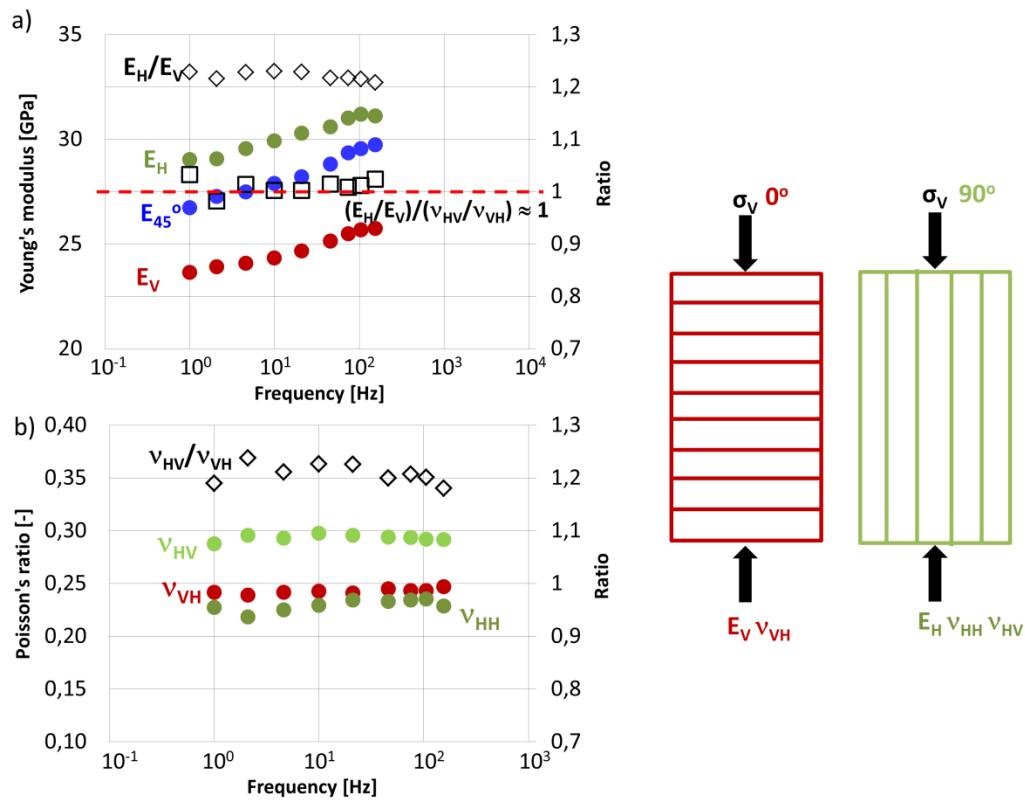
Figure 4: Young's moduli and Poisson's ratios (closed symbols) measured with 0°, 45° and 90°-oriented Mancos shale samples (as received) at seismic frequencies. The measurements were done at a confining stress of 17 MPa, an axial stress of 26 MPa, and zero pore pressure. Open symbols show the ratios ν_{HV}/ν_{VH} and E_H/E_V, as well as the ratio of the ratios, $(E_H/E_V)/(\nu_{HV}/\nu_{VH})$, that for TI symmetry should be equal to 1.
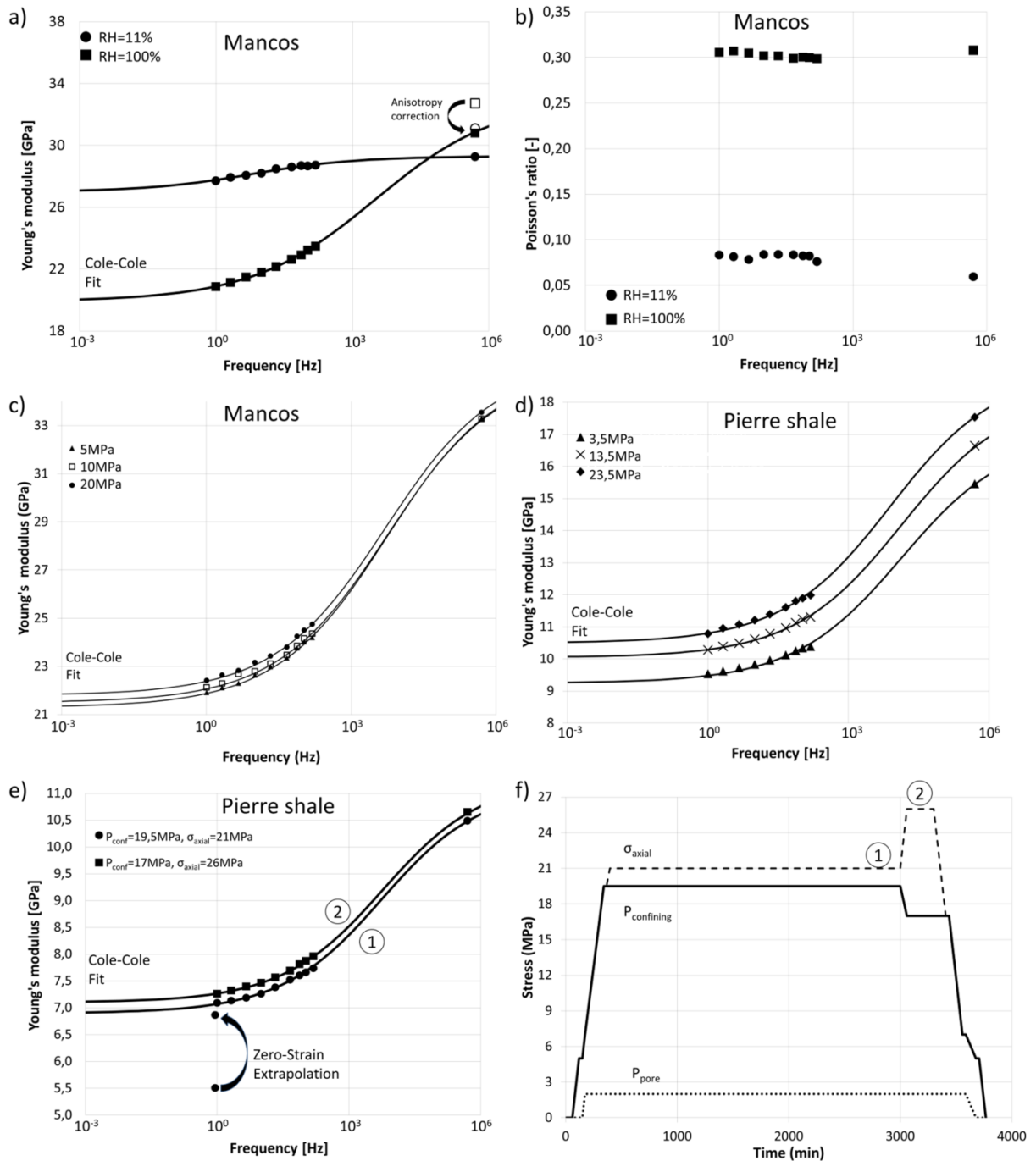
Figure 5: Demonstrations of different applications of the new experimental setup for seismic dispersion measurements: (a,b) Young's moduli, E_V (a) and Poisson's ratio, ν_{VH} (b) as a function of frequency for partially saturated Mancos shale. The samples were stabilized in environments of 11% and 100% relative humidity (RH), respectively, and measured under 17MPa confining stress and 26MPa axial stress. (c) Stress sensitivity of Young's modulus, E_V, of Mancos shale (as received) at seismic and ultrasonic frequencies for hydrostatic loading (5, 10, and 20 MPa) at a constant additional axial stress of 2 MPa. (d) Stress sensitivity of Young's modulus, E_V, of partially saturated Pierre shale (stabilized in 75% RH) at seismic and ultrasonic frequencies for hydrostatic loading (3.5, 13.5, and 23.5 MPa) at a constant additional axial stress of 1,5 MPa. (e) Impact of constant-mean-stress loading on the Young's modulus, E_V, of fully saturated Pierre shale at seismic and ultrasonic frequencies. The stress path used in this experiment is shown in (f). Also shown in (e) is the static Young's modulus obtained from triaxial unloading, and the zero-strain extrapolation of the static Young's modulus (Fjær et al. 2013). Solid lines in (a-e) show manual Cole-Cole fits to the experimental data (Cole and Cole 1941).